Two-dimensional convex-molecule fluid model for surface adsorption of proteins: Effect of soft interaction on adsorption equilibria

Paritosh Mahata and Sovan Lal Das*
Department of Mechanical Engineering, Indian Institute of Technology Kanpur, Kanpur 208016, India
(Received 12 July 2014; published 19 December 2014)

Adsorption of proteins on membrane surfaces plays an important role in cell biological processes. In this work, we develop a two-dimensional fluid model for proteins. The protein molecules have been modeled as two-dimensional convex and soft particles. The Lennard-Jones potential for circular particles and Kihara (12,6) potential for elliptical particles with hard core have been used to model pairwise intermolecular interactions. The equation of state of the fluid model has been derived using Weeks-Chandler-Andersen decomposition and it involves three parameters, an attraction, a repulsion, and a size parameter, which depend on the shape and core size of the molecules. For validation of the model, a two-dimensional molecular dynamics simulation has been performed. Finally, the model has been applied to study the adsorption of proteins on a flat membrane. In comparison with the existing model of hard and convex particles for protein adsorption, our model predicts a higher packing fraction for the adsorption equilibria. Although the present work is based on Lennard-Jones-type interaction, it can be extended for other specific soft interactions between convex molecules. Thus the model has general applicability for any other two-dimensional adsorption systems of molecules with soft interaction.

DOI: 10.1103/PhysRevE.90.062713 PACS number(s): 87.10.−e, 87.14.ep, 87.15.kt, 87.16.D−

I. INTRODUCTION

Most cell biological processes depend on adsorption or binding of proteins to membrane surfaces. Malfunctioning of this adsorption may lead to disorder in subsequent downstream processes. Thus it is of great interest to researchers to understand the mechanism for adsorption of proteins or proteinlike biomolecules. It includes mainly specific or nonspecific interactions between proteins and surfaces. For example, antibodies and polypeptide hormones with particular epitopes or receptors found on the surface of the cell membrane are responsible for localization of the protein molecules [1]. Also, in other cases, nonspecific electrostatic or hydrophobic interactions lead to the nonlocalized adsorption of proteins onto lipid bilayer membranes [2]. Between these two cases, the latter class of interactions is less studied, but important for several cell biological functions such as association of soluble proteins with membranes, formation of multienzyme complexes, and curvature sorting of protein molecules.

There are two types of theoretical model proposed in the literature for the nonspecific adsorption of biomolecules to surfaces. The first class of models are similar to lattice models of gas adsorption [3,4]. The surface of the membrane is divided into a large number of virtual sites and one adsorbed ligand can occupy one or more sites. The second class of models [5,6] use a continuum model of hard-particle fluids [7] to calculate the chemical potential of the adsorbed ligand. In a similar approach, Chatelier and Minton [8] have calculated adsorption isotherms of proteins of various shapes on a planar surface using scaled particle theory (SPT) [9,10]. The adsorbed phase of the protein was modeled as a two-dimensional hard-particle fluid.

Recently, the adsorbed phase of proteins has been modeled as a two-dimensional van der Waals or Bragg-Williams gas to study the curvature sorting of proteins on a cylindrical lipid membrane [11,12]. The hard repulsive behavior of the molecules for both these models and the other hard-particle fluid models does not capture reality well. Further, the curvature-generating or -sensing peripheral membrane proteins typically do not have a circular geometry. For example, the projections of the membrane-binding BAR domain of amphiphysin and NBAR domains of endophilin onto membranes have elongated shapes [13,14].

In this work, we develop a two-dimensional fluid model for soft convex molecules and, subsequently, apply it to study the adsorption of proteins on a flat membrane. As a starting point we consider a Lennard-Jones-type interaction between the protein molecules. The Lennard-Jones interaction can be replaced by more refined and accurate protein-protein interactions, if available. The size and shape of the binding domain of the protein molecules have been approximated by two-dimensional convex molecules. We derive the equation of state using the well-known Weeks-Chandler-Andersen (WCA) decomposition theory [15–17] in which the potential was decomposed into a repulsive and an attractive part at the minimum energy depth. This is a perturbation theory, where the repulsive part is taken to be the reference system and the attractive part of the potential is considered to be a small perturbation. Thus the unperturbed or reference system is composed of soft repulsive particles.

We first consider a system of circular particles with Lennard-Jones (LJ) interaction and use the radial distribution function obtained from the scaled particle theory [9,10] to model the soft repulsive region of the WCA decomposition. Subsequently, we derive the equation of state for convex elliptical molecules. Since the LJ potential cannot be directly used for elliptical molecules due to the dependence of the interaction parameters on the orientation, we employ the Kihara (12,6) potential. Instead of the center-to-center distance, the potential is defined in terms of the shortest core-to-core distance between the molecules and it has the same algebraic form as the LJ potential. Here, we have used the radial distribution function for a hard-convex-body system

*Corresponding author: sovandas@iitk.ac.in

given by Boublik [18]. The equation of state thus obtained is simple and involves three parameters: one for attraction, one for repulsion, and a size parameter that depends on a shape parameter and a core parameter. The shape parameter measures the deviation from a circular shape and the core parameter signifies the hard region of the convex molecule. The equation of state derived for elliptical molecules encompasses the circular molecule system as a special case.

The WCA decomposition was earlier used by Steele [19] for a two-dimensional Lennard-Jones fluid made of circular disks to study monolayer adsorption on a flat solid surface. The adsorption isotherm is calculated from the configuration integral modeled by a reference system composed of the WCA fluid and the corresponding effective hard-disk diameter was computed based on a Taylor series expansion of the cavity function. In our work, the low-density behavior has been captured by the terms up to the second virial coefficient in the equation of state. The second virial coefficient is exact for the LJ potential. Second, the high-density behavior of the fluid is treated by use of the reference potential of the WCA decomposition. We do not compute the effective hard-disk diameter explicitly; instead, the effective excluded area was obtained by relating the second virial coefficient to the parameters of the van der Waals gas model. In addition to this, we have extended our work for two-dimensional system of convex particles.

We also carry out a two-dimensional molecular dynamics simulations using the LAMMPS code and compare the results from our theory with the simulation results. We consider an isothermal-isobaric (*NPT*) ensemble, and the interaction between particles is modeled via the LJ potential for circular particles and the Gay-Berne potential [20–24] for elliptical particles. The Gay-Berne potential models the anisotropic LJ interaction between the convex molecules. The agreement between theoretical and simulation results is very good for the circular-particle system. For the elliptical particles we choose the aspect ratio to be 3:1 as the parameters in the potential were readily available for this ratio. Furthermore, the Gay-Berne potential is not the same as the Kihara (12,6) potential and a quantitative comparison between the theory and simulation has not been attempted.

Finally, we study the biophysical system of protein adsorption on a flat lipid bilayer membrane surface. The interaction free energy of proteins bound to the membrane surface has been derived from our theoretical model. The results from our model were compared with the hard-convex-particle model of Chatelier and Minton [8]. In our case, the binding isotherm deviates from their work towards the Langmuir isotherm. This implies that the proteins are overlapping with each other due to their soft interaction on the membrane surface. This is also a more realistic behavior.

II. EQUATION OF STATE

In this section, we derive the equation of state for a two-dimensional convex-molecule fluid model based on a statistical-mechanical approach. First, a two-dimensional (2D) model of circular particles with Lennard-Jones interaction was developed. Subsequently, we extend the model for elliptical particles. Since the LJ potential cannot be directly applied to convex particles that are noncircular, we use the Kihara (12,6) potential for elliptical particles.

A. Circular-disk particles with LJ interaction

We consider a system of N circular-disk particles in an area A and at a constant temperature T. The pressure equation is written in terms of the radial distribution function $g(r)$ under the assumption of pairwise additivity of the intermolecular potential [15],

$$\frac{p}{\rho kT} = 1 - \frac{\rho}{4kT}\int_0^\infty g(r)\left(r\frac{du(r)}{dr}\right)2\pi r dr, \qquad (1)$$

where p is the pressure, k is the Boltzmann constant, ρ ($= N/A$) is the number density, r is the center-to-center distance between two particles, and $u(r)$ defines the intermolecular potential. For our case $u(r)$ is the LJ potential.

$$u(r) = 4\epsilon\left[\left(\frac{\sigma}{r}\right)^{12} - \left(\frac{\sigma}{r}\right)^{6}\right], \qquad (2)$$

where σ is the effective diameter of the particles, for which the potential is zero, and ϵ is the minimum depth of the potential.

The integral of Eq. (1) can be split up into the second virial coefficient B_2 and an integral I in terms of the cavity function $y(r) = e^{\beta u(r)}g(r)$ [25],

$$\frac{p}{\rho kT} = 1 + \rho B_2 + \rho I, \qquad (3)$$

where

$$B_2 = -\frac{1}{4}\int_0^\infty \beta e^{-\beta u(r)}\left(r\frac{du(r)}{dr}\right)2\pi r dr$$
$$= \pi\int_0^\infty (1 - e^{-\beta u(r)})r dr \qquad (4)$$

and

$$I = \frac{1}{4}\int_0^\infty r f(r)[y(r) - 1]2\pi r dr, \qquad (5)$$

in which $f(r) = -\beta\frac{du(r)}{dr}e^{-\beta u(r)}$ and $\beta = 1/kT$.

The second virial coefficient is calculated from Eq. (4) and it is also possible to find it experimentally. Since we compute it exactly for the Lennard-Jones potential, the terms up to the second virial coefficient in Eq. (3) are sufficient to describe the low-density behavior of the fluid. Due to the lack of a suitable analytical expression for $g(r)$ for the LJ potential, it is not possible to get an analytical expression for the integral I. However, the integral I is dominated by the repulsion of the molecules [25] and it is evaluated from the repulsive part of the LJ potential of the WCA decomposition [16,17]. So we can expect that the integral I should be negligible for low density. A suitable algorithm for the radial distribution function of the hard-disk fluid is proposed in the high-density regime as follows.

In the WCA decomposition, the repulsive or unperturbed part of the LJ potential is defined as

$$u_0(r) = \begin{cases} u(r) + \epsilon & \text{for} \quad r < r_m, \\ 0 & \text{for} \quad r \geqslant r_m, \end{cases}$$

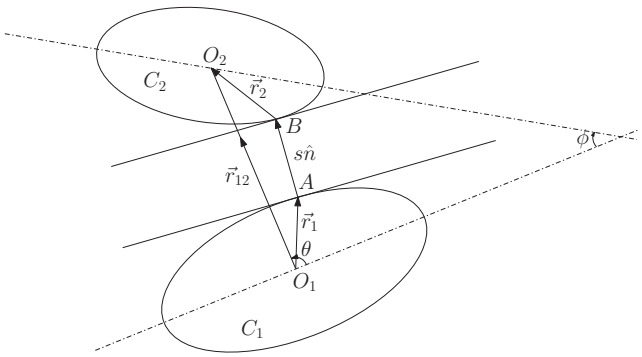

FIG. 1. Geometry of two convex bodies with the shortest envelope-to-envelope distance s [18].

where $r_m = 2^{1/6}\sigma$ corresponds to the minimum of the potential. Then the repulsive contributions to the functions $f(r)$ and $y(r)$ become

$$f_0(r) = \begin{cases} -\beta \frac{du_0}{dr} e^{-\beta u_0} & \text{for } r < r_m, \\ 0 & \text{for } r \geqslant r_m, \end{cases} \tag{6}$$

and

$$y_0(r) = e^{\beta u_0} g(r). \tag{7}$$

All these expressions approximate the integral I as

$$I \approx \frac{1}{4} \int_0^{r_m} r f_0(r)[y_0(r) - 1] 2\pi r dr. \tag{8}$$

For spherical particles, the function $y(r)$ is smoothly decreasing, and $f_0(r)$ is sharply peaked in the repulsive region of the potential (see Fig. 1 of Ref. [25]). Simulation results show a similar behavior [26]. For circles they are expected to behave in the same way as the potential is the same. Thus $y_0(r)$ in Eq. (8) can be replaced by the radial distribution function of a hard-disk fluid at contact. Finally, the equation of state (3) becomes

$$\frac{p}{\rho kT} = 1 + \rho B_2 + J\rho[(G(\eta) - 1], \tag{9}$$

where $B_2(T)$ is the second virial coefficient,

$$J(T) = \frac{1}{4} \int_0^{r_m} r f_0(r) 2\pi r dr = \pi \int_0^{r_m} (1 - e^{-\beta u_0}) r dr, \tag{10}$$

is a scaling factor that measures the contribution of the hard-disk fluid, and $G(\eta)$ is the radial distribution function of a hard-disk fluid in terms of the packing fraction η of the system of particles. The packing fraction is defined as $\eta = b\rho/2$ with b being half of the excluded area of the particle.

Now, a suitable choice of a radial distribution function $G(\eta)$ will complete the specification, and we choose from SPT analysis [9,10]

$$G(\eta) = \frac{1 - \frac{\eta}{2}}{(1 - \eta)^2}. \tag{11}$$

Drawing an analogy with a van der Waals gas [25], and using the repulsive part of the potential in the WCA decomposition, half of the excluded area b of a particle is expressed as

$$b(T) = B_2 + T \frac{dB_2}{dT} = \pi \int_0^{r_m} [1 - (1 + \beta u_0) e^{-\beta u_0}] r dr. \tag{12}$$

Note that $B_2(T)$ depends on the full intermolecular potential (i.e., the LJ potential), whereas $J(T)$ and $b(T)$ depend only on the repulsive part of the WCA decomposition. We now introduce two parameters $a_a = J - B_2$ and $a_r = J$ and rewrite the equation of state (9) as

$$\frac{p}{\rho kT} = 1 - a_a \rho + a_r \rho \frac{(4 - \rho b)}{(2 - \rho b)^2}. \tag{13}$$

In the above, a_a signifies the interaction parameter based on attraction and a_r is based on soft repulsion of the WCA decomposition. Finally, the equation of state (13) contains three parameters—two interaction parameters and one size parameter. The details about these parameters are discussed in Sec. II C after extending the above formulation for a system of elliptical particles.

B. Elliptical-disk particles with the Kihara (12,6) potential

For a system of elliptical-disk particles, both the intermolecular potential u and the radial distribution function g depend on the position and relative angular orientation of the particles. For example, σ and ϵ used in the LJ potential depend on the angular orientation [Eq. (2)] between the interacting particles. This makes the derivation of an equation of state difficult. To overcome this difficulty, the potential is expressed in terms of the shortest core-to-core distance s instead of the center-to-center distance r_{12} (see Fig. 1). A Kihara core-type potential has been used for this purpose [18,27–29]. The pressure equation (1) for the system of elliptical-disk particles is written as

$$\frac{p}{\rho kT} = 1 - \frac{\rho}{4kT} \int_0^1 \int_0^\infty g(r_{12}, \omega) \left(r_{12} \frac{\partial u(s)}{\partial r_{12}} \right) dr_{12} d\omega, \tag{14}$$

where $u(s)$ is the Kihara core-type intermolecular potential defined in terms of s, and $\omega = \phi/2\pi$ denotes the normalized relative orientation between the interacting particles. To consider the Lennard-Jones type of interaction between the elliptical particles, we use the Kihara (12,6) potential,

$$u(s) = 4\epsilon_K \left[\left(\frac{\sigma_K}{s} \right)^{12} - \left(\frac{\sigma_K}{s} \right)^{6} \right], \tag{15}$$

where σ_K is the shortest effective core-to-core distance, for which the potential is zero, and ϵ_K is the minimum depth of the potential. We consider assumed parallel hard convex cores to the molecules.

Since, we do not consider the effect of the relative angular orientation for the interaction parameters, the present Kihara model represents the isotropic behavior of the fluid based on the shortest core-to-core distance. The effect of angular orientation for a three-dimensional Kihara fluid was considered by Cuetos *et al.* [30] to study liquid-crystal phase behavior.

We rewrite Eq. (14) in terms of s as

$$\frac{p}{\rho kT} = 1 - \frac{\rho}{2kT}\int_0^\infty \frac{\partial u(s)}{\partial s} g_{av}(s) A_{1+s+2}(s) ds, \quad (16)$$

where A_{1+s+2} is the area excluded by the molecules in maintaining the shortest core-to-core distance s with the other molecules [18], and the average distribution function $g_{av}(s)$ is given by [28]

$$g_{av}(s) = \frac{1}{2A_{1+s+2}}\int_0^{2\pi}\int_0^1 g(s,\theta,\omega)\vec{r}_{12}\cdot\left(\frac{\partial \vec{r}_{12}}{\partial\theta}\times\hat{b}\right)d\theta d\omega.$$

The average cavity function, $y_{av}(s) = e^{\beta u(s)} g_{av}(s)$ in this case is assumed to have the same qualitative behavior as the average cavity function for circular particles. Then Eq. (16) can be expressed in the same form as Eq. (9) for circular particles, except that the expressions for the second virial coefficient B_2 and the scaling factor J for the Kihara core system [27] will differ from those for circular particles. When all the molecules have the same shape and size the quantities B_2 and J become

$$B_2(T) = (\alpha+1)A_c + \pi\int_0^\infty (1 - e^{-\beta u})(2R_c + s) ds, \quad (17)$$

$$J(T) = (\alpha+1)A_c + \pi\int_0^{s_m} (1 - e^{-\beta u_0})(2R_c + s) ds, \quad (18)$$

where $s_m = 2^{1/6}\sigma_K$ is the shortest core-to-core distance between the molecules, for which the Kihara (12,6) potential is minimum. The geometric parameter R_c multiplied by 2π denotes the circumference and A_c is the area of the core [18]. $G(\eta)$ is the radial distribution function for the system of hard convex particles. We have used the expression for $G(\eta)$ obtained by Boublik [18] using SPT,

$$G(\eta) = \frac{1 - \frac{1}{\alpha+1}\eta}{(1-\eta)^2}, \quad (19)$$

where $\eta = \rho b/(\alpha+1)$ is the packing fraction and $\alpha = \pi R_c^2/A_c$ is the shape parameter of the core. The expression for $G(\eta)$ is remarkably accurate in the repulsive region and consistent with the circular particles for $\alpha = 1$. Note that it is also possible to use other expressions for $G(\eta)$ [31].

Finally, the equation of state for the elliptical particles is written in the form of Eq. (13), so that

$$\frac{p}{\rho kT} = 1 - a_a\rho + a_r\rho\frac{(\alpha+1)^2 - \rho b}{[(\alpha+1) - \rho b]^2}, \quad (20)$$

where a_a and a_r, similar to those in Eq. (13), denote the attraction and repulsion parameters, respectively. The size of the molecule is given by

$$b(T) = (\alpha+1)A_c + \pi\int_0^{s_m}[1 - (1+\beta u_0)e^{-\beta u_0}](2R_c + s) ds.$$

Since the shape parameter of the core is introduced in the equation of state (20), we can write $\sigma_K = \sigma$ and $\epsilon_K = \epsilon$, where σ and ϵ are the parameters for the LJ potential. Then the present thermodynamic model for elliptical particles can be obtained from an equivalent system of circular particles having circular cores. For $\alpha = 1$ and a zero core size of the molecules, the above equation reduces to the equation of state (13) for the system of circular particles. Thus the equation of state derived here for the elliptical-particle system encompasses the circular-particle system with LJ interaction as well. Also, Eq. (20) represents the Kihara model for circular particles with $\alpha = 1$ and a valid core.

Upon introducing a reduced density $\rho^* = \rho\sigma^2$ and a reduced pressure $p^* = p\sigma^2/\epsilon$ we rewrite Eq. (20) in dimensionless form

$$\frac{p^*}{T^*} = \rho^* - a_a^*\rho^{*2} + a_r^*\rho^{*2}\frac{(\alpha+1)^2 - \rho^* b^*}{[(\alpha+1) - \rho^* b^*]^2}, \quad (21)$$

where $T^* = 1/\beta\epsilon$ is the reduced LJ temperature, and a_a^*, a_r^*, and b^* are the dimensionless attraction, repulsion, and size parameters, respectively. They are

$$a_a^* = \frac{a_a}{\sigma^2} = \pi\int_0^{2^{1/6}}\left(1 - e^{-[4(x^{-12}-x^{-6})+1]/T^*}\right)(z+x)dx - \pi\int_0^\infty\left(1 - e^{-4(x^{-12}-x^{-6})/T^*}\right)(z+x)dx, \quad (22)$$

$$a_r^* = \frac{a_r}{\sigma^2} = \frac{\pi}{4}\left(\frac{\alpha+1}{\alpha}\right)z^2 + \pi\int_0^{2^{1/6}}\left(1 - e^{-[4(x^{-12}-x^{-6})+1]/T^*}\right)(z+x)dx, \quad (23)$$

and

$$b^* = \frac{b}{\sigma^2} = \frac{\pi}{4}\left(\frac{\alpha+1}{\alpha}\right)z^2 + \pi\int_0^{2^{1/6}}\left(1 - \left(1 + \frac{4(x^{-12}-x^{-6})+1}{T^*}\right)e^{-[4(x^{-12}-x^{-6})+1]/T^*}\right)(z+x)dx, \quad (24)$$

where $x = s/\sigma$ is the reduced core-to-core distance and $z = 2R_c/\sigma$ is the core parameter.

The core parameter represents the ratio of the radius of the circular hard core to the half thickness of the circular particles above the core. Furthermore, the core parameter significantly influences the repulsive behavior of the system of particles. We can use this parameter to fit the present model for any desired pressures and temperatures. Note that the above equation of state is valid mathematically up to the reduced density $\rho^* = (\alpha+1)/b^*$.

C. Discussion of the parameters $a_a(T)$, $a_r(T)$, and $b(T)$

The parameters a_a, a_r, and b and their reduced forms given by Eqs. (22) through (24) depend on temperature. Variations of these parameters with temperature have been shown in

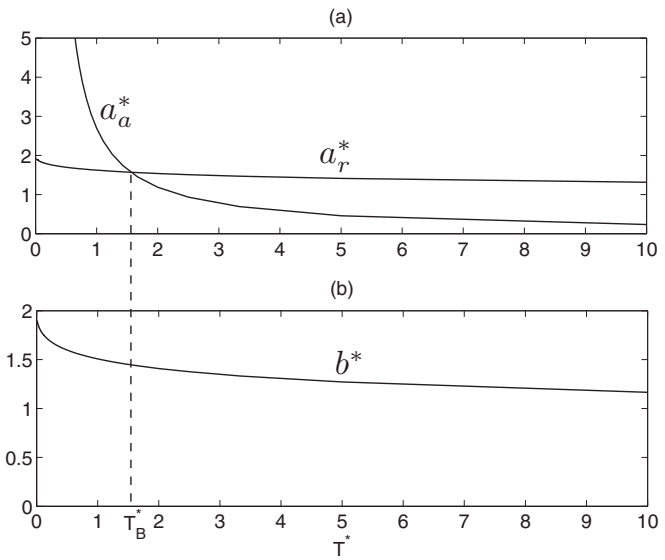

FIG. 2. Variations of reduced model parameters (a) a_a^* and a_r^* and (b) b^* with respect to the reduced LJ temperature T^* for the system of circular particles ($\alpha = 1$). All quantities are dimensionless.

Figs. 2 and 3 for the systems of circular and elliptical particles, respectively. For both cases, it is observed that the attraction parameter a_a^* dominates over the repulsive parameter a_r^* below the Boyle temperature T_B^* [where $B_2(T) = 0$]. This implies that at low temperatures the behavior of the pressure equation (20) is characterized by the attraction parameter a_a^* and at high temperatures it is characterized by the repulsion parameter a_r^* for a given density. The half excluded area of the molecules b^* decreases with temperature as shown in Figs. 2(b), 3(c), and

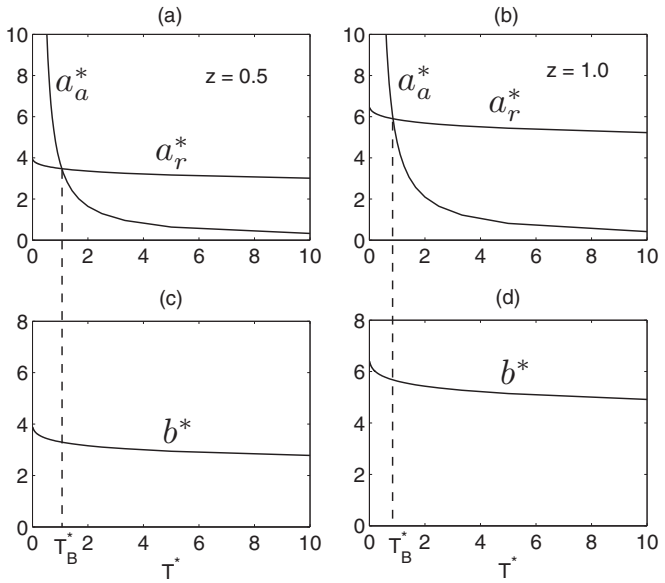

FIG. 3. Variations of reduced model parameters a_a^* and a_r^* (a) for $z = 0.5$, (b) for $z = 1.0$; and of the size parameter b^* (c) for $z = 0.5$, (d) for $z = 1.0$ with respect to the reduced LJ temperature T^* for the system of elliptical particles with axial ratio 3:1. All quantities are dimensionless.

TABLE I. Values of Boyle parameters for a system of elliptical particles (axial ratio 3:1) and different values of z. The shape parameter $\alpha = 1.51$ for axial ratio 3:1.

z	$T_B^* = kT_B/\epsilon$	$a_B^* = a_B/\sigma^2$	$p_B^* = p_B\sigma^2/\epsilon$
0	1.560	1.681	0.928
0.1	1.403	2.119	0.663
0.2	1.282	2.604	0.493
0.3	1.186	3.135	0.378
0.4	1.107	3.731	0.297
0.5	1.042	4.367	0.238
0.6	0.985	5.076	0.195
0.7	0.937	5.814	0.161
0.8	0.895	6.623	0.135
0.9	0.858	7.519	0.115
1.0	0.826	8.403	0.098

3(d). This effect is manifested by a reduction in the packing fraction of the system with increasing temperature.

For the system of elliptical particles, the above parameter values increase with the core parameter z as shown in Fig. 3. Also, the Boyle parameters such as the Boyle temperature T_B, Boyle area a_B, and Boyle pressure p_B vary with z. These parameters are obtained from the following relations [25]:

$$B_2(T_B) = 0, \quad a_B = T_B \left(\frac{dB_2}{dT}\right)_{T_B}, \quad p_B = \frac{kT_B}{a_B}, \tag{25}$$

and are listed in Table I for different values of z.

In common practice, the intermolecular potential parameters σ and ϵ are chosen by fitting the experimentally obtained variation of the second virial coefficient B_2 with temperature around the Boyle temperature T_B. Then the parameters a_a, a_r, and b (or a_a^*, a_r^*, and b^*) are no longer fitting parameters, but universal parameters of the system and their values depend on temperature. The quantity T_B and consequently the corresponding σ and ϵ are fixed for a given model.

D. Critical temperature and density

The reduced critical temperature T_c^* and density ρ_c^* of the present equation of state are obtained from the following two relations:

$$\left(\frac{\partial p^*}{\partial \rho^*}\right)_{\rho_c^*, T_c^*} = 0 \quad \text{and} \quad \left(\frac{\partial^2 p^*}{\partial \rho^{*2}}\right)_{\rho_c^*, T_c^*} = 0.$$

For the system of circular particles ($\alpha = 1, z = 0$) we obtain $\rho_c^* = 0.27$ and $T_c^* = 0.668$. The critical constants for the system of elliptical particles depend on the core parameter z and they are given in Table II. Note that, unlike the Boyle parameters, the critical density and temperature depend on the shape parameter α for zero core ($z = 0$).

III. OTHER THERMODYNAMIC FUNCTIONS

In the following, we compute other thermodynamic functions such as the Helmholtz free energy, activity coefficient, and internal energy using our present model. For comparison we also carry out molecular simulations which are discussed in Sec. IV.

TABLE II. Values of critical constants for a system of elliptical particles for axial ratio 3:1 with different values of z.

z	$\rho_c^* = \rho_c\sigma^2$	$T_c^* = kT_c/\epsilon$
0	0.305	0.700
0.1	0.251	0.648
0.2	0.211	0.608
0.3	0.180	0.575
0.4	0.156	0.548
0.5	0.137	0.525
0.6	0.121	0.505
0.7	0.107	0.488
0.8	0.096	0.473
0.9	0.087	0.459
1.0	0.079	0.447

A. Helmholtz free energy

The Helmholtz free energy (F) is defined as

$$F = U - TS, \tag{26}$$

where U is the internal energy and S is the entropy of the system. The excess Helmholtz free energy (F^{ex}) relative to the ideal gas at the same temperature and density is obtained by integrating the equation of state within the limits 0 and ρ,

$$\frac{F^{ex}}{NkT} = -a_a\rho + \frac{a_r\alpha\rho}{(\alpha+1)-\rho b} - \frac{a_r}{b}\ln(1-\rho A_m). \tag{27}$$

The reduced excess free energy $F^{ex*} = F^{ex}/\epsilon$ in terms of the other reduced quantities is

$$\frac{F^{ex*}}{NT^*} = -a_a^*\rho^* + \frac{\alpha a_r^*\rho^*}{(\alpha+1)-b^*\rho^*} - \frac{a_r^*}{b^*}\ln\left(1-\frac{\rho^* b^*}{\alpha+1}\right). \tag{28}$$

For an ideal gas at the same temperature and density, we have the Helmholtz free energy

$$\frac{F^{id}}{NkT} = \ln(\rho A_m) - 1. \tag{29}$$

Then the absolute free energy of the system of particles is written in terms of the packing fraction $\eta = \rho A_m$,

$$\frac{F}{NkT} = \ln\eta - (\alpha+1)\frac{a_a}{b}\eta + \alpha\frac{a_r}{b}\left(\frac{\eta}{1-\eta}\right) - \frac{a_r}{b}\ln(1-\eta) - 1. \tag{30}$$

B. Activity coefficient of the fluid

The activity coefficient is the measure of nonideality of the mixing of liquid and gas phases of the fluid. It depends on the concentration of the molecules in the liquid phase of the fluid. It is determined from the chemical potential of the system of particles, so that

$$\frac{\mu}{kT} = \frac{1}{kT}\left(\frac{\partial F}{\partial N}\right)_{A,T} = \mu_0 + \ln(\lambda\eta), \tag{31}$$

where μ_0 is the standard state chemical potential and λ is the activity coefficient of the fluid. Since we consider the chemical potential in terms of the change of free energy from a reference system we neglect μ_0. Then in reduced form we have

$$\ln\lambda = -2(\alpha+1)\frac{a_a^*}{b^*}\eta + \alpha\frac{a_r^*}{b^*}\frac{\eta}{(1-\eta)^2} + \alpha\frac{a_r^*}{b^*}\frac{\eta}{1-\eta} - \frac{a_r^*}{b^*}\ln(1-\eta). \tag{32}$$

C. Internal energy

The reduced excess internal energy relative to the ideal gas for the same temperature and density is obtained by differentiating Eq. (28) with respect to temperature,

$$\frac{U^{ex*}}{NT^*} = A_a\rho^* - \frac{[(\alpha+1)-b^*\rho^*]\alpha A_r\rho^* + \alpha a_r^* B\rho^{*2}}{[(\alpha+1)-b^*\rho^*]^2} - \frac{a_r^*}{b^*}\frac{B\rho^*}{(\alpha+1)-b^*\rho^*} + \frac{b^*A_r - a_r^*B}{b^{*2}} \times \ln\left(1-\frac{b^*\rho^*}{\alpha+1}\right), \tag{33}$$

where A_a, A_r, and B are the products of the derivatives of a_a^*, a_r^*, and b^* with respect to T, respectively.

IV. SIMULATION DETAILS

To validate the theoretical model developed in the previous section, a 2D molecular dynamics simulation has been performed using the LAMMPS code. The molecules are considered as LJ particles for circles and Gay-Berne particles for ellipses with aspect ratio 3:1. We considered the Lennard-Jones potential for circular particles and the Kihara (12,6) potential for elliptical particles in our theoretical model; they are isotropic in nature. In the simulation we use the Gay-Berne potential [20–24] as the Kihara (12,6) type of potential is not available for elliptical particles in LAMMPS. The Gay-Berne potential is based on the center -to-center distance and can represent anisotropic interaction behavior. It also resembles the LJ potential for the circular particles.

A. Simulation parameters

The simulation parameters are chosen as the default values of the LAMMPS package for most of the cases. The dimensions of the parameters are taken in distance units (σ), energy units (ϵ), and mass units (m). The molecules are modeled as finite-size spherical particles with mass $1m$ and diameter 1σ. For 2D simulations, LAMMPS has an option to zero out the z-dimension velocity and force on each atom of the simulation box lying in the x-y plane. The cutoff radius and neighbor-list radius of the LJ potential are taken as 2.5σ and 2.8σ, respectively.

An isothermal-isobaric (NPT) ensemble of molecular dynamics simulations has been carried out for a 200×200 sq lattice (total 40 000 particles) for 5×10^5 time steps. The average values of the last 2×10^5 time steps with a gap of 1000 time steps have been considered as our thermodynamic outputs. The standard deviation of those output data has been checked and it is always below 1%. The time step of each run has been taken as 0.005τ ($\tau = \sigma[m/\epsilon]^{1/2}$) and the pressure $P = P^*\epsilon/\sigma^3$, where P^* is the nondimensional pressure. The thermostat and barostat damping have been set at 0.5τ.

For the excess-free-energy calculation, an *NPT* ensemble of 3×10^5 time steps was performed first to equilibrate the system. Then another 3×10^5 time steps are run for the *NVT* ensemble by changing the strength of the LJ potential by multiplying with a prefactor ξ. The ξ values are taken as 0.1,0.2,0.3, . . . ,1.0. For each ξ, the *NVT* ensemble average of the derivative of the potential energy with respect to ξ has been obtained by averaging the simulation data of the last 2×10^5 time steps with a gap of 1000 time steps. The excess free energy is then computed from the relation [32]

$$F^{ex} = \int_0^1 \left\langle \frac{\partial U}{\partial \xi} \right\rangle_\xi d\xi, \tag{34}$$

where $\langle \frac{\partial U}{\partial \xi} \rangle_\xi$ is the *NVT* ensemble average of the derivative of the potential energy U with respect to ξ for a given ξ.

In the following, we compare our theoretical results with the results obtained from molecular simulations for the circular-particle system. We observe very good quantitative agreement between theory and simulation for the circular-particle system. For the elliptical-particle system, the theoretical variations of the thermodynamic functions with density match qualitatively the results obtained from simulations (not shown). Due to the mismatch in the potentials used in the theory and available in LAMMPS, we do not attempt a quantitative comparison.

B. Simulation results and discussion for circular-particle system

For $\alpha = 1$ and $z = 0$, Eqs. (21), (33), and (28) represent pressure, excess internal energy, and excess free energy, respectively, as functions of the reduced density for a system of circular particles. Their variations with reduced density for different temperatures, along with the simulation results, are presented in Figs. 4 and 5. All the simulation data are taken above the critical temperature ($T_c^* = 0.668$). The agreement between theory and simulation is very good for the pressure and excess internal energy. The agreement for excess internal energy gets better with increasing temperature as shown in Fig. 5: it matches at least up to the critical density for $T^* = 0.75$ as shown in Fig. 5(a), at least up to twice the critical density for T^* above 1.1 [Figs. 5(b) and 5(c)]. The match between theory and simulation is reasonably good for the variation of the excess free energy. The agreement is quite good even above the critical density as shown in Fig. 5(a). Agreement is poor around the Boyle temperature ($T_B^* = 1.56$). This is due to the fact that the term I in Eq. (3) is not accurate nor can it be neglected around the Boyle temperature. Still, our theory predicts the behavior of the fluid system at least up to the critical density for all temperatures. At higher temperatures, the present model is accurate for the excess free energy in the regime of low to high density as shown in Fig. 5(d). Considering the fact that the perturbation theories have acceptable accuracy at high temperatures [19], the present model has reasonable accuracy even at low temperatures.

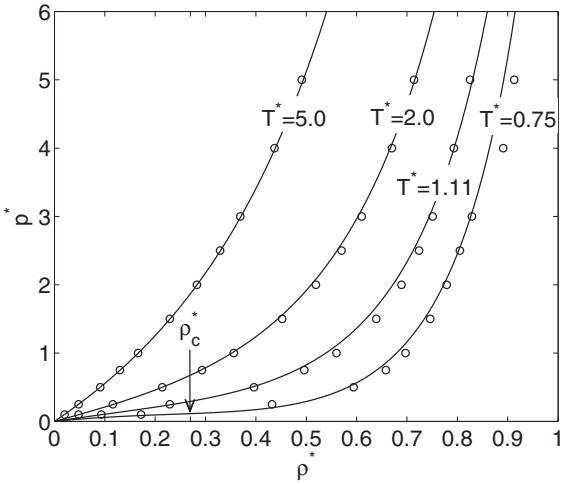

FIG. 4. Comparison between theoretical and simulation results for circular particles for the variations of reduced pressure with reduced density for different temperatures. The solid lines and circles represent theoretical and simulation results, respectively. All quantities are dimensionless.

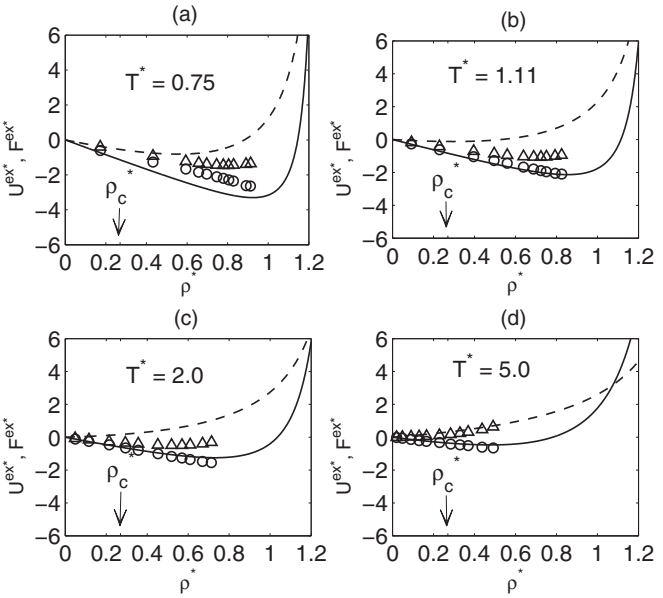

FIG. 5. Comparison between theoretical and simulation results for circular particles for the variations of the reduced excess internal energy (solid lines for theory and circles for simulation) and excess free energy (dashed lines for theory and triangles for simulation) with reduced density for different temperatures as mentioned. All quantities are dimensionless.

Note that the approximation used for the cavity function $y(r)$ in the formulation is not expected to be very accurate in the critical region [25]. Still, we obtain good agreement in comparison with simulation data for thermodynamic functions like the pressure, excess internal energy, and excess free energy near the critical density even for $T^* = 0.75$ which is close to the critical temperature $T_c^* = 0.668$. The simulation results for pressure, excess internal energy, and excess free energy are also presented in Table III.

V. ADSORPTION OF PROTEINS ONTO A FLAT MEMBRANE SURFACE: AN APPLICATION

In this section, we apply the theoretical model developed in Secs. II and III to study adsorption of proteins on a flat membrane surface in contact with a protein reservoir

TABLE III. Simulation data for pressure, excess internal energy, and excess free energy obtained from different temperatures for a system of circular particles.

$T^* = 0.75$				$T^* = 1.11$			
p^*	ρ^*	U^{ex*}	F^{ex*}	p^*	ρ^*	U^{ex*}	F^{ex*}
0.10	0.172	−0.604	−0.397	0.10	0.093	−0.268	−0.177
0.25	0.432	−1.263	−0.920	0.25	0.229	−0.622	−0.422
0.50	0.594	−1.666	−1.223	0.50	0.396	−1.032	−0.706
0.75	0.658	−1.849	−1.329	0.75	0.496	−1.283	−0.863
1.00	0.697	−1.965	−1.384	1.00	0.560	−1.451	−0.949
1.50	0.746	−2.113	−1.431	1.50	0.639	−1.666	−1.031
2.00	0.779	−2.210	−1.447	2.00	0.689	−1.799	−1.058
2.50	0.805	−2.282	−1.446	2.50	0.724	−1.891	−1.063
3.00	0.829	−2.352	−1.434	3.00	0.751	−1.956	−1.050
4.00	0.891	−2.608	−1.383	4.00	0.793	−2.042	−1.004
5.00	0.913	−2.635	−1.347	5.00	0.825	−2.092	−0.941
$T^* = 2.0$				$T^* = 5.0$			
0.10	0.048	−0.109	−0.063	0.10	0.020	−0.027	0.004
0.25	0.116	−0.258	−0.147	0.25	0.048	−0.071	0.010
0.50	0.214	−0.472	−0.259	0.50	0.091	−0.135	0.024
0.75	0.293	−0.646	−0.341	0.75	0.130	−0.194	0.041
1.00	0.356	−0.788	−0.400	1.00	0.166	−0.246	0.064
1.50	0.452	−1.003	−0.464	1.50	0.229	−0.337	0.118
2.00	0.519	−1.156	−0.483	2.00	0.283	−0.412	0.180
2.50	0.570	−1.267	−0.478	2.50	0.329	−0.473	0.244
3.00	0.610	−1.353	−0.457	3.00	0.369	−0.526	0.322
4.00	0.670	−1.470	−0.389	4.00	0.437	−0.603	0.473
5.00	0.714	−1.540	−0.303	5.00	0.491	−0.652	0.637

(solution). The proteins in the solution were considered to behave as an ideal gas. The proteins adsorbed onto the membrane were treated as a 2D soft-convex-particle fluid. Earlier, Chatelier and Minton [8] studied the system, using SPT, and considering the adsorbed proteins as hard convex particles.

For equilibrium the chemical potentials of proteins in solution and on the membrane surface should be the same. For any given protein concentration c in solution we have

$$\mu_{\text{soln}} = \mu_{\text{surf}}, \tag{35}$$

where $\mu_{\text{soln}} = \mu_{\text{soln},0} + kT \ln c$ and μ_{surf} are the chemical potentials of the proteins in solution and on the surface, respectively. The surface-protein chemical potential μ_{surf} is given by Eq. (31) with $\mu_0 = \mu_{\text{surf},0}/kT$. Here, $\mu_{\text{soln},0}$ and $\mu_{\text{surf},0}$ denote the standard state chemical potentials for the solution and surface, respectively. Finally, the binding isotherm is given by

$$Kc = \lambda\eta, \tag{36}$$

where $K = \exp[-(\mu_{\text{surf},0} - \mu_{\text{soln},0})/kT]$ and λ is the activity coefficient obtained from Eq. (32).

In Fig. 6, we compare the binding isotherms for the circular-particle system with LJ interaction (for $\alpha = 1$ and $z = 0$), obtained from our model [Eq. (36)] and Chatelier and Minton's SPT [8] for different temperatures. We obtain a higher packing fraction than Chatelier and Minton. This is due to the soft interaction between the protein molecules considered in our

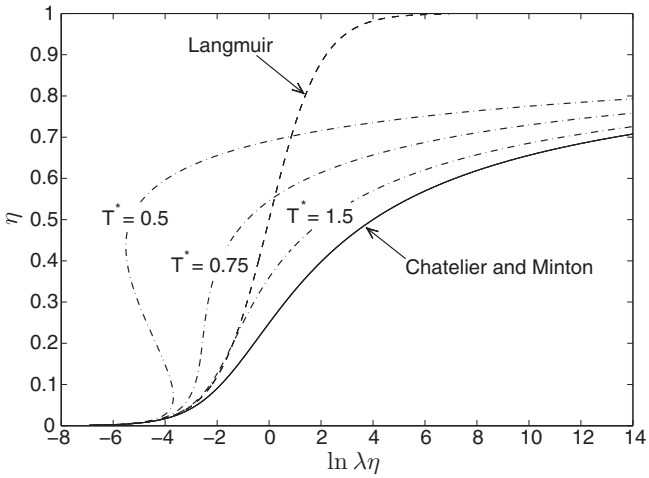

FIG. 6. Binding isotherms of protein (circular) adsorption on a flat surface from the present model [$\alpha = 1$ and $z = 0$ in Eq. (32)], the Chatelier and Minton [8] model, and the Langmuir isotherm. The dash-dotted lines are based on our model for different temperatures. All quantities are dimensionless.

work. With increasing temperature the isotherms from our model approach the isotherm of Chatelier and Minton. At low temperatures the adsorption isotherm is steeper than the Langmuir isotherm [3] at low density (or packing fraction). This suggests that attraction between the molecules works at a low density. With increasing packing fraction, the repulsive effect between the molecules starts dominating. This broadens the adsorption isotherm from the Langmuir isotherm. Finally, the excluded-area effect of the molecules leads the isotherm to match that of Chatelier and Minton for high temperatures. At very high temperatures (not shown in the figure), there is a small discrepancy between the isotherms from our model and those of Chatelier and Minton. The different formulation (WCA perturbation theory) used here leads to a different

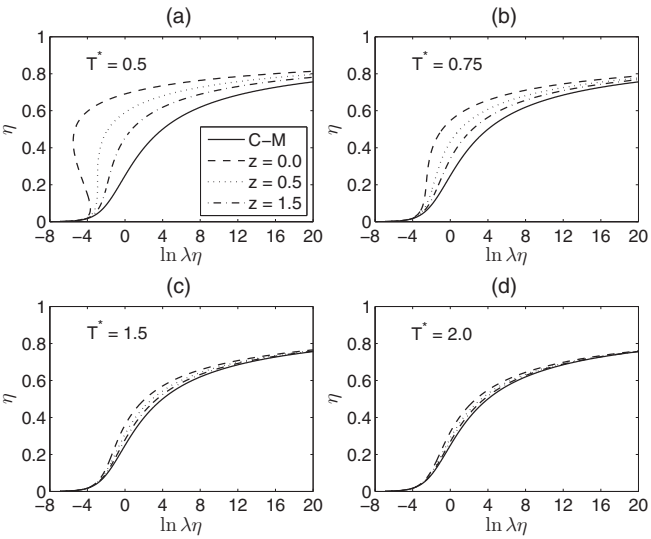

FIG. 7. Binding isotherms of protein (circular) adsorption from the present model and the Chatelier and Minton [8] model for different core sizes (z) and temperatures. All quantities are dimensionless.

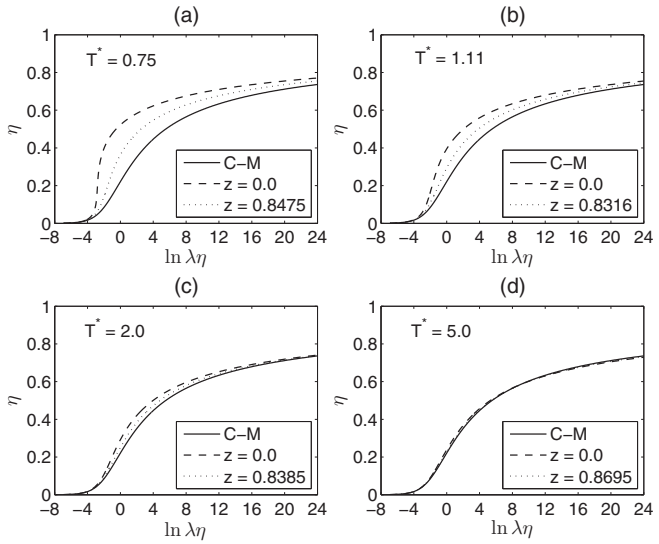

FIG. 8. Binding isotherms from the present model and the Chatelier-Minton model [8] for a system of elliptical particles (axial ratio 3:1) for different core sizes (z) and temperatures. All quantities are dimensionless.

excluded area compared to that obtained by Chatelier and Minton. Note also that multiple values of the packing fraction have been observed below the critical temperature, suggesting that the protein phases differ in density. Such behavior has also been observed by Singh *et al.* [11] for sorting of proteins in a cylindrical membrane tube.

We now compare the binding isotherms with the SPT results (Chatelier and Minton), for circular particles with nonzero core, for different values of the core parameter z and at a few temperatures. The results are shown in Fig. 7. With increasing z the isotherms broaden towards that of Chatelier and Minton. This is a quite natural result from our model as the excluded-area effect of the molecules increases with increasing core size. However, even for large core sizes, there will always be a soft-repulsive-interaction film of thickness σ between the molecules. Similar behavior has also been observed for the system of elliptical particles with a Kihara core potential as shown in Fig. 8. We obtained higher packing fraction values than Chatelier and Minton even at the best-fit value of z (with the simulation data) due to soft interactions between the molecules. Thus we can say that the present theoretical model efficiently captures the convex as well as the soft nature of proteinlike biomolecules. Note that a comparison with experiments will be the best possible validation of the model. However, comparison with Chatelier and Minton's work does bring out the essential features of the soft particle-particle interaction. We aim to apply the model to protein adsorption on a lipid bilayer membrane and extract model parameters through fitting in future work.

VI. CONCLUSIONS

In this work, we have developed a two-dimensional convex-molecule fluid model with soft interaction for proteins adsorbed on membranes. The Lennard-Jones interaction for circular particles and the Kihara core (12,6) potential for elliptical particles were used to model soft interaction between the proteins. Comparison of our model with molecular dynamics simulation results for thermodynamic functions like the pressure, excess free energy, and excess internal energy has shown good quantitative agreement for circular-particle systems and qualitative agreement for elliptical-particle systems. The model developed here has been applied to study protein binding on the surface of a flat biomembrane. Binding isotherms from the present model have been compared with the isotherms from hard- and convex-molecule fluid model. As expected, we have obtained a higher packing fraction value in the adsorption isotherm in comparison to that obtained from the hard- and convex-molecule fluid model. This is more realistic behavior of soft molecules such as adsorbed proteins. The great advantage of the present model is that the size of the core of the molecules controls both the attraction and repulsion parameters. It helps to fit the model with any desired pressure and temperature of the system. This enhances the applicability of the model to various other two-dimensional adsorption systems comprised of soft molecules.

ACKNOWLEDGMENTS

The authors acknowledge the High Performance Computing (HPC) facility at IIT Kanpur where the molecular simulations were carried out. This work was supported by IIT Kanpur, Grant No. IITK/ME/20090343, Department of Science and Technology, Government of India, Grant No. DST/ME/20120003, and in part by the Project of Knowledge Innovation Program (PKIP) of Chinese Academy of Sciences, Grant No. KJCX2.YW.W10. The authors would also like to thank the anonymous referees for pointing out the issue of mismatch between the Kihara (12,6) and Gay-Berne interaction potentials.

[1] P. M. Conn, *The Receptors*, Vol. 1 (Academic Press, Orlando, FL, 1984).
[2] M. B. Sankaram and D. Marsh, in *Protein-Lipid Interactions*, edited by A. Watts (Elsevier, Amsterdam, 1993), p. 127.
[3] K. A. Dill and S. Bromberg, *Molecular Driving Forces: Statistical Thermodynamics in Biology, Chemistry, Physics, and Nanoscience* (Garland Science, New York, 2010).
[4] S. Stankowski, Biochim. Biophys. Acta **735**, 352 (1983).
[5] S. Stankowski, Biochim. Biophys. Acta **777**, 167 (1984).
[6] L. K. Tamm and I. Bartoldus, Biochemistry **27**, 7453 (1988).
[7] F. C. Andrews, J. Chem. Phys. **64**, 1941 (1976).
[8] R. C. Chatelier and A. P. Minton, Biophys. J. **71**, 2367 (1996).
[9] H. L. Frisch, Adv. Chem. Phys. **6**, 229 (1964).
[10] H. Reiss, Adv. Chem. Phys. **9**, 1 (1965).

[11] P. Singh, P. Mahata, T. Baumgart, and S. L. Das, Phys. Rev. E **85**, 051906 (2012).
[12] C. Zhu, S. L. Das, and T. Baumgart, Biophys. J. **102**, 1837 (2012).
[13] C. Mim, H. Cui, J. A. Gawronski-Salerno, A. Frost, E. Lyman, G. A. Voth, and V. M. Unger, Cell **149**, 137 (2012).
[14] A. Frost, V. M. Unger, and P. D. Camilli, Cell **137**, 191 (2009).
[15] D. A. McQuarrie, *Statistical Mechanics* (Viva Books, New Delhi, 2008).
[16] J. D. Weeks, D. Chandler, and H. C. Andersen, J. Chem. Phys. **54**, 5237 (1971).
[17] J. D. Weeks, D. Chandler, and H. C. Andersen, J. Chem. Phys. **55**, 5422 (1971).
[18] T. Boublik, Mol. Phys. **29**, 421 (1975).
[19] W. A. Steele, J. Chem. Phys. **65**, 5256 (1976).
[20] J. G. Gay and B. J. Berne, J. Chem. Phys. **74**, 3316 (1981).
[21] W. M. Brown, M. K. Petersen, S. J. Plimpton, and G. S. Grest, J. Chem. Phys. **130**, 044901 (2009).
[22] R. Everaers and M. R. Ejtehadi, Phys. Rev. E **67**, 041710 (2003).
[23] R. Berardi, A. Constantini, L. Muccioli, S. Orlandi, and C. Zannoni, J. Chem. Phys. **126**, 044905 (2007).
[24] R. Berardi, A. P. J. Emersont, and C. Zannoni, J. Chem. Soc. Faraday Trans. **89**, 4069 (1993).
[25] Y. Song and E. Mason, J. Chem. Phys. **91**, 7840 (1989).
[26] L. Verlet, Phys. Rev. **165**, 201 (1968).
[27] T. Boublik, Mol. Phys. **27**, 1415 (1974).
[28] T. Boublik, Mol. Phys. **51**, 1429 (1984).
[29] T. Boublik, Mol. Phys. **32**, 1737 (1976).
[30] A. Cuetos, B. Martnez-Haya, S. Lago, and L. F. Rull, Phys. Rev. E **68**, 011704 (2003).
[31] Y. Song and E. A. Mason, Phys. Rev. A **42**, 4743 (1990).
[32] D. M. Eike and E. J. Maginn, J. Chem. Phys. **124**, 164503 (2006).